JTTEE5 19:484–494
DOI: 10.1007/s11666-009-9413-3
1059-9630/$19.00 © ASM International

Ultrafine Particulate Dispersed High-Temperature Coatings by Hybrid Spray Process

P.S. Mohanty, A.D. Roche, R.K. Guduru, and V. Varadaraajan

(Submitted April 24, 2009; in revised form August 3, 2009)

Oxide dispersion strengthened alloys (ODS), although not commonly used in coating applications, have long been used for high-temperature structural applications due to their superior creep properties. In this paper, we present the design, synthesis, and characterization of a new class of functionally engineered high-temperature coatings in which ultrafine oxide particulates are dispersed in the matrix alloy to achieve superior creep resistance along with improved high-temperature corrosion and erosion resistance. These coatings were fabricated using a novel technique called "hybrid spray process". Hybrid spray technique combines arc spray and high-velocity oxy fuel (HVOF) spray processes; the metallic matrix alloys are fused by the wire arcing component of the process, whereas the ultrafine particles are synthesized in-flight by the HVOF component from liquid precursors. These particulate dispersed high-temperature composite coatings were fabricated using liquid precursors for SiO_2, Cr_2O_3, Al_2O_3, and wire feed stock of 55/45 NiCr, in one step. The coatings were then characterized using electron microscopy (SEM/TEM) and thermogravimetric analysis (TGA). High-temperature erosion, oxidation, and corrosion performance of these coatings were also evaluated and compared with 304 stainless steel, arc sprayed NiCr coatings as well as Alloy 625 overlay cladding. The hybrid spray process produced dense coatings with uniform dispersion of the ultrafine oxide particles. Further, these coatings also demonstrated superior corrosion, erosion, and oxidation resistance; SiO_2 particulate dispersion being most effective in terms of high-temperature corrosion resistance.

Keywords Al_2O_3, engineered coatings, hybrid spray, NiCr alloy, SiO_2, ultrafine oxide dispersion

1. Introduction

High-temperature coatings are ubiquitous to industrial power generation, marine applications, and aircraft propulsion systems. Most high-temperature coatings operate under extremely harsh conditions with conflicting operational requirements. For instance, coatings used in power plant boilers need to ensure an effective protection against high-temperature corrosion under oxidizing, sulfidizing, carburizing environments and erosion from fly ash, as well as having a high thermal conductivity to exchange heat in order to provide an effective and economical maintenance. Further, to avoid premature failure, high-temperature coatings also require good adhesion to the substrate, minimal mismatch in coefficient of thermal expansion (CTE) between the coating and the substrate material, good thermal fatigue and creep resistance (Ref 1-5).

Most commercial coating systems lack all the required attributes for a given environment. For example, thermal sprayed NiCr (55/45 wt.%) alloy is usually recommended for erosion-corrosion protection for boiler tubes in power generation applications (Ref 6-9). Weld overlay coatings of Alloy 625 (Ni-21Cr-9Mo-3.5Nb) have also been used for this application. When nickel is alloyed with chromium (>15 wt.%), Cr oxidizes to Cr_2O_3, which could make it suitable for use up to about 1200 °C (Ref 10), although in practice its use is limited to temperatures below about 800 °C. The efficacy of NiCr coatings deteriorates severely when molten ash deposits consisting of sodium-potassium-iron tri-sulfates $(Na,K)_3Fe(SO_4)_3$ are present. Further, higher Cr content also reduces the creep resistance of NiCr alloys. Particularly, this issue becomes magnified in the case of thermal spray coatings. In addition to the grain boundaries, presence of splat boundaries, an inherent feature in thermal sprayed coatings, also contributes to poor creep performance at very high temperatures through sliding (Ref 11, 12).

The continued pursuit for increased efficiency in power generation and propulsion systems led to the development

This article is an invited paper selected from presentations at the 2009 International Thermal Spray Conference and has been expanded from the original presentation. It is simultaneously published in *Expanding Thermal Spray Performance to New Markets and Applications: Proceedings of the 2009 International Thermal Spray Conference*, Las Vegas, Nevada, USA, May 4-7, 2009, Basil R. Marple, Margaret M. Hyland, Yuk-Chiu Lau, Chang-Jiu Li, Rogerio S. Lima, and Ghislain Montavon, Ed., ASM International, Materials Park, OH, 2009.

P.S. Mohanty, A.D. Roche, R.K. Guduru, and **V. Varadaraajan**, Additive Manufacturing Process Laboratory (AMPL), University of Michigan-Dearborn, 4901 Evergreen Road, Dearborn, MI 48128. Contact e-mail: rkguduru@umd.umich.edu.

of functionally engineered coatings with multiple attributes. For example, an alternative method of combating the effects of coal ash corrosion is to install a material that contains sufficient amount of oxide stabilizing elements such as aluminum or silicon (NiCrAl, NiCrBSi NiCrMoBSi, and NiCrBSiFe) to resist the dissolution of the oxide film when the molten ash is deposited. Similarly, functionally gradient materials (FGM) were proposed (Ref 13) to obtain multifunctional properties with a combination of different metallic and ceramic systems in an engineered fashion. These materials were found to be very promising candidates for high-temperature applications because of the reduced thermal stresses between the interfaces, resulting in enhanced thermal fatigue life (Ref 14). The high-temperature creep strength of metals also greatly improved by the addition of a high-temperature stable dispersoid phases, due to grain boundary pinning such as the oxide dispersion strengthened super alloys (Ni-ThO_2 and NiCr-ThO_2) (Ref 15). A number of nanostructured coating systems exist that have demonstrated superior oxidation and erosion properties (Ref 16). These coatings can be categorized into (a) ceramic coatings (nano-ZrO_2-7 wt.% Y_2O_3; Ref 16), (b) combination of metallic and ceramic powders (NiCr-Cr_2C_3; Ref 17) and (c) microcrystalline metallic matrix with embedded nanoparticles (NiCr-Y_2O_3; Ref 18). Particles smaller than 200 nm generally integrate well with the matrix, which is key to the excellent creep properties of nanoparticulate composites (Ref 19). Among the above systems, materials containing coarse grain structures with nanosized ceramic dispersoids are found to be the best choice for highly improved creep strength (Ref 20). This composite concept, i.e., coatings consisting of nanosized dispersoids in a matrix, is investigated in this study.

Various approaches have been adopted to disperse second phase particulates into bulk matrix phase, such as mechanical alloying/powder metallurgy (Ref 19), in situ formation of dispersoids via a chemical reaction within the matrix phase (Ref 21), spray synthesis (Ref 22), casting techniques (Ref 23), and electrodeposition (Ref 24). Processing methods, such as powder metallurgy (Ref 25-29) and thermal spraying (Ref 30-34), cannot easily tailor the composition in a functional manner. Typically, thermal sprayed composite coatings are made using premixed powders with a given ratio of the constituent phases. This limits the production as well as the design flexibility. Further, a spray deposition approach involving direct spraying of nanosized powders has a number of limitations (Ref 35, 36). The primary issue is the introduction of nanosized powders into the high-velocity thermal spray jet and their impingement on the substrate. Nanosized powders tend to agglomerate, resulting in plugged particle feed line, and the extremely small particles do not readily penetrate the jet. Also, impingement on to the substrate is difficult as the small powders follow the gas streamlines. An alternative methodology is to introduce a liquid or gaseous precursor, which reacts in flight to form nanosized particles (Ref 16, 35). This approach is very promising and has worked well for several material systems. Combustion synthesis using liquid precursors has been used to deposit a number of different high-temperature oxide coatings, including Al_2O_3, Cr_2O_3, SiO_2, CeO_2, some spinel oxides ($MgAl_2O_4$, $NiAl_2O_4$), and yttria stabilized zirconia (YSZ) (Ref 37). For example, using a solution of aluminum acetylacetonate in ethanol, alumina was deposited at temperatures of approximately 850, 1050, and 1250 °C (Ref 38). Similarly, SiO_2 has been deposited by combustion synthesis of ethanol containing tetrathyloxysilicate precursor.

As for the production of nanoparticle dispersed microcrystalline coating by thermal spray technique, different approaches have been adopted such as agglomeration of nanosized particles with a binder, used in the Co-WC cermet (Ref 36), or premixing of dispersoid phase with the matrix powder (Ref 39-41). However, these approaches also suffer from the same design inflexibility mentioned above. This paper presents an innovative approach to synthesize ultrafine/nano particulate dispersed (Al_2O_3, SiO_2) NiCr alloy coatings. A novel process called ''hybrid spray technique'' (Ref 42) has been employed to fabricate these functionally engineered coatings in a single step. The rational behind the selection of the dispersoid phases, their liquid precursors, and the particulate distribution layout is presented. The influence of these dispersoid phases on the high-temperature characteristics of the resulting coatings is discussed in detail.

2. Experiments

The ''hybrid spray'' process utilized in this study was conceptualized in our laboratory at the University of Michigan (Ref 42, 43). This process combines the arc and HVOF spray techniques; molten metal at the arcing tip is atomized and rapidly propelled to the substrate by a HVOF jet. This so-called ''hybrid'' concept shown in Fig. 1 offers many advantages. The process offers all benefits of wire stock and productivity of electric arc spraying combined with noticeably improved coating density of HVOF. In addition to introducing material through arcing mechanism, if desired, powder/liquid/gas precursors can also be fed through the HVOF coaxial feed line (Fig. 1a). This enables us to tailor the composition *inflight* by introducing particles into the HVOF jet, to cater to specific property requirements of a composite coating or an FGM. This unique capability completely eliminates the necessity of processing and handling of the ultrafine particulates prior to feeding them into the hybrid gun. Synthesizing and introducing ultrafine and nano dispersoids inflight in a functional manner to produce FGM coatings by the hybrid technique is quite unique in terms of simplicity compared to any other processes. A comparative picture of the steps involved in processing of particulate reinforced composites by conventional routes versus our approach is presented in Table 1.

Table 2 lists the liquid precursors employed for the synthesis of the dispersoid phase particles. The rationale behind the selection of the dispersoids (SiO_2 and Al_2O_3)

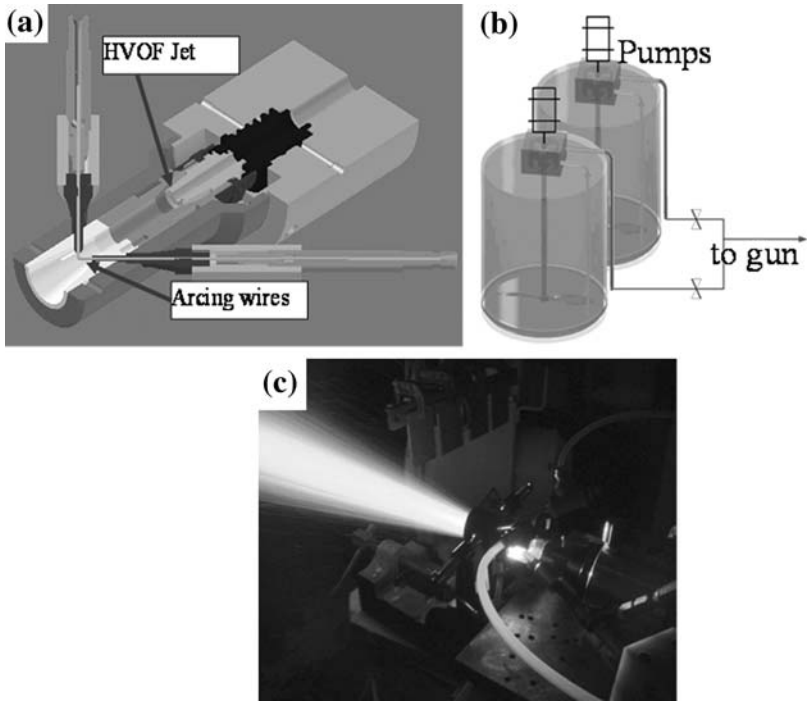

Fig. 1 (a) Schematic of hybrid gun, (b) hybrid gun in operation, and (c) precursor feeding system

Table 1 Process comparison

Conventional routes			
Liquid route	**Powder met route**	**Common spray route**	**Hybrid spray route**
Matrix/dispersoid phase ↓ Melting/mixing ↓ Cast & solidify ↓ Composite	Matrix/dispersoid phase ↓ Mechanical mixing ↓ Compact/sinter ↓ Composite	Matrix/dispersoid powders ↓ Mechanical mixing ↓ Co-spray mixed powders	Matrix wire/dispersoid precursor ↓ Melt & atomize wires for matrix and melt/synthesize dispersoid ↓ Co-deposit composite

Table 2 List of precursors used

Target material	Precursor materials	Percentage
NiCr-matrix	NiCr wire	55/45 wt.%
Al_2O_3 particulate	Aluminum nitrate – $Al(NO_3)_3{\cdot}9H_2O$	1:1 by weight in isopropyl alcohol (70%)
Cr_2O_3 stabilizer	Chromium nitrate – $Cr(NO_3)_3{\cdot}9H_2O$	Up to 50% by weight of aluminum nitrate
SiO_2 particulate	Tetraethoxysilane	100%

and their influence on the properties either in combination or as an individual component is shown as follows:

- The silica particles are expected to provide both creep and crack resistance. It has also been demonstrated that the presence of SiO_2 enhances the high-temperature resistance of chromia scale (Ref 44, 45).
- The presence of alumina is expected to provide enhanced high-temperature corrosion resistance. Also, the introduction of SiO_2 into alumina-based coatings has been found to form mullite and reduce the cracking within the coating (Ref 46). Mullite is known for its excellent creep resistance (Ref 47, 48).
- It has also been found that the presence of chromia aids in α-alumina formation as well as limits the phase transformations during heating to temperatures below 1200 °C (Ref 46, 49). Therefore, chromium nitrate was added to the aluminum nitrate precursor to stabilize the α-alumina phase. Both precursors being nitrate could be mixed into a single reservoir.

Following the above-mentioned approach of in-flight synthesis, different oxide ceramic particles were introduced into the NiCr (55/45 wt.%) alloy coating. Prior to developing NiCr FGM coatings, only particle synthesis was carried out and then particles were collected with an electrostatic precipitator to analyze their size and shape.

Subsequently, the following coatings were deposited onto mild steel coupons for characterization: (a) Al_2O_3, (b) $Cr_2O_3Al_2O_3$, (c) SiO_2, (d) NiCr only, (e) NiCr + Cr_2O_3, (f) NiCr + Al_2O_3, (g) NiCr + SiO_2, and (h) FGM coating with combination of NiCr, SiO_2, and Cr_2O_3-Al_2O_3 as shown in Fig. 2. Along with these coatings, NiCr coatings using twin wire arc spray process (TAFA 3830, Praxair Surface Technologies, Indianapolis, IN) were also deposited for comparison purposes. The arc current and voltage for both the processes were kept at 100 A and 36 V, respectively. The HVOF gas pressures were maintained at 50/65/80 psi of propylene/oxygen/air, respectively. The aluminum nitrate and tetraethoxysilane precursors were fed from separate reservoirs as shown in Fig. 1(b); however, they mixed together prior to the injection into the combustion jet. The atomization of the liquid was achieved by a two-fluid injector. Liquid precursors up to 100 cm^3/min were fed to the HVOF jet coaxially.

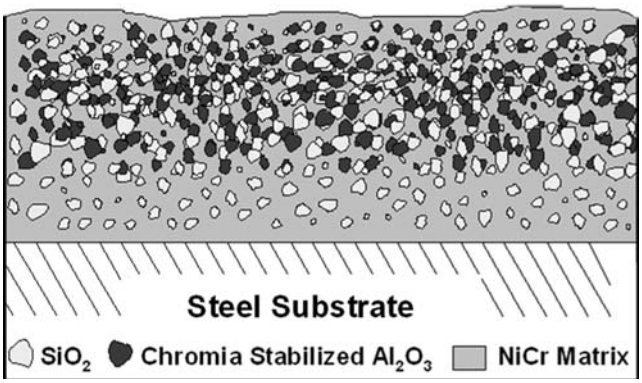

Fig. 2 FGM coating design

Microstructural analysis of the coatings was done using electron microscopy (SEM/TEM). The oxidation characteristics of the coatings were characterized on a TA instruments SDT Q600 model for thermogravimetric analysis (TGA). For functional property characterization, coatings were tested for hot erosion, wet corrosion, and hot corrosion and compared with 304 stainless steel as well as alloy 625 overlay cladding. The hot erosion test setup consisted of a grip for holding and rotating (80 rpm) the coated samples while heating with a heat source (HVOF flame), and an alumina grit (250 mesh) delivering system at a fixed angle (45°) as shown in Fig. 3(a). The flow rate of the grit was 60 g/min and the applied grit carrier air pressure was 15 psi at a rate of 42 SCFM. Testing was done at 750 °C for 3 min on spray-coated cylinders. Wet corrosion tests were done at room temperature in a dilute 0.1% NaCl solution. NiCr coatings sprayed by the hybrid and arc techniques were tested using an electrochemical cell shown in Fig. 3(b). Electrochemical experiments were performed using a Solartron (Hampshire, UK) SI 1287 potentiostat at the open circuit potential for two different time periods (0 and 24 h). Hot corrosion tests were carried out by applying film of sulfates and chlorides (potassium, sodium, and iron) onto the surface of coated samples (304 stainless steel caps) as shown in Fig. 3(c). Samples were first weighed. Then, the surface of the samples was coated with a solution of sulfate/chloride and water mixed in a weight ratio of 1:1—the sample was carefully masked to ensure salt solution only covered the sprayed coating—the area coated with salt solution was also measured. The solution was dried to leave a film of salt on the surface of the sample. The masking material was removed and the sample was weighed again. Samples were then placed in an oven at 900 °C for 24 h. This test also included samples of bare 304 stainless steel cap as well as alloy 625 overlay cladding. After the hot corrosion test, weight loss/gain of

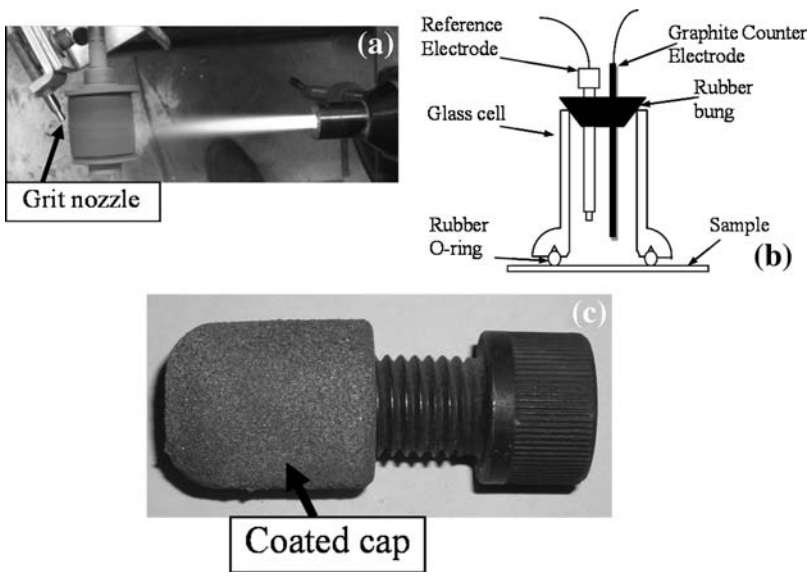

Fig. 3 (a) Hot erosion test set up, (b) corrosion cell, and (c) sample for hot corrosion test

the samples was measured to evaluate the corrosion resistance.

3. Results and Discussion

The atomization of the liquid precursor prior to the injection into the combustion jet plays an important role on the size as well as on the distribution of the particles in the final coating. The requirements for the atomization system include controlled and uniform flow, ability to operate against a back pressure of 30 psi pressure that exists in HVOF flame at the point of injection, and the ability to generate mono-dispersed micron-sized droplets.

Four methods for nebulizing the liquid precursors were investigated. These included a syringe delivery method, a mixing block into which high-pressure air and liquid precursor were fed, a single ultrafine hole through which the precursor was forced under high pressure and a two-fluid atomization system. Among them, the two-fluid approach delivered the most consistent results. The working principle involves a high-velocity air flow exerting a drag force on a slow flowing velocity liquid, thus nebulizing the liquid stream. The resulting droplet stream is shown in Fig. 4(a). Further, side (Fig. 4b) as well as axial injection (Fig. 4c) into the combustion jet was also investigated. In the case of side injection, all the droplets were not captured in the flame and a large proportion of droplets arrived at the substrate without being pyrolyzed. With axial injection the atomized droplets are created inside the HVOF gun at the position where powder particles are normally introduced. As expected, all of the precursor material were captured and pyrolized in the flame. The oxide particles (Al_2O_3, SiO_2) synthesized from liquid precursors were collected using an electrostatic precipitator for analysis. Figure 5(a) shows an atomic force microscope (Quesant, Q-Scope 350) image of a fine SiO_2 particle collected by an electrostatic precipitator. Most collected particles were very fine and their size ranged from a few nanometers to several hundred nanometers. The size distribution of alumina particles collected on the precipitator is shown in Fig. 5(b). As can be seen, in addition to the small particles, clusters were also observed. Energy dispersive x-ray (EDX) analysis of the particles confirmed the composition. In general, silica particles were the finest compared to the alumina as well as chromia stabilized alumina particles which is reflected in the SEM picture of oxide coatings presented in Fig. 6. Addition of chromium nitrate to aluminum nitrate increased the cluster size as shown in Fig. 6(b). Also, some large bubble-shaped features with internal voids were formed in this coating. However, silica particles were uniform and fine exhibiting a characteristic cluster pattern as shown in Fig. 6(c).

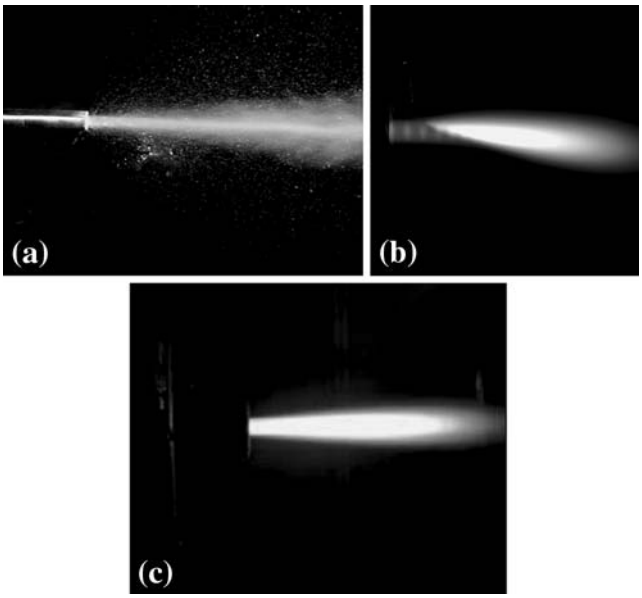

Fig. 4 Liquid precursor injection: (a) atomization, (b) side injection, and (c) axial injection

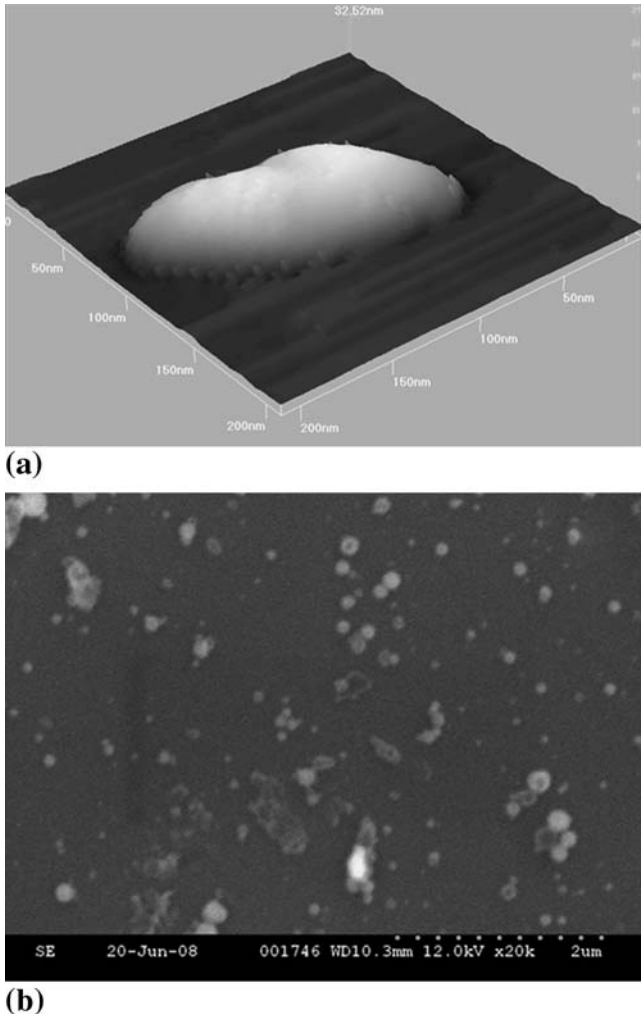

Fig. 5 (a) AFM image of SiO_2 particle (200 × 200 nm) and (b) SEM picture of collected alumina particles

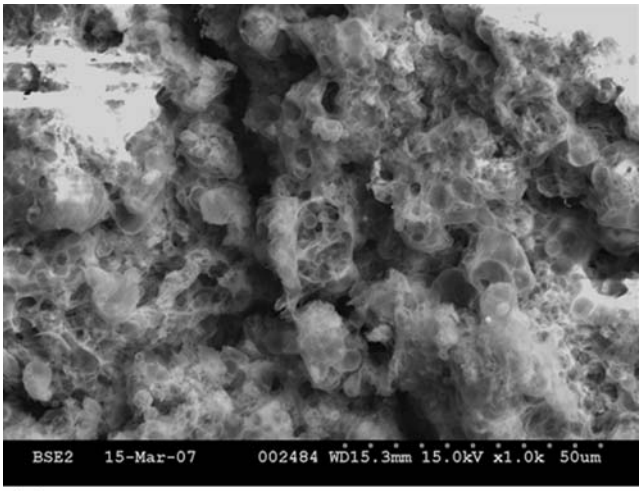

(a)

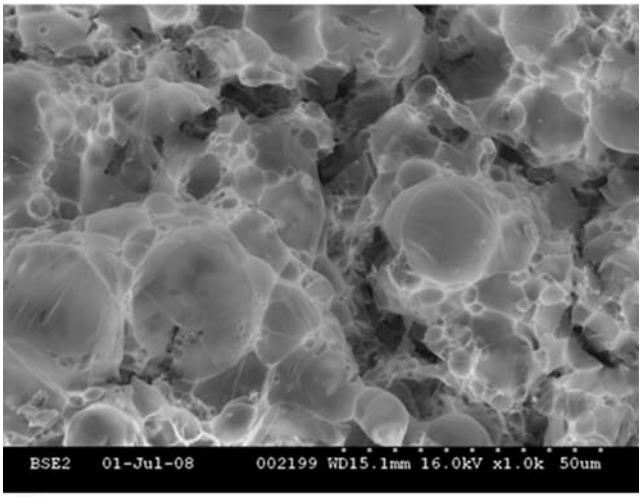

(b)

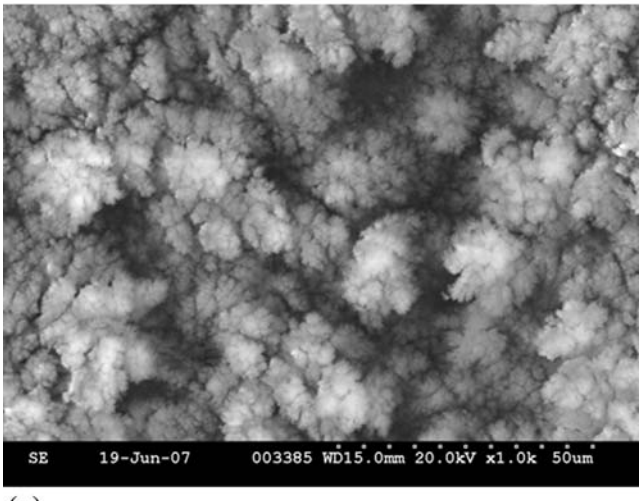

(c)

Fig. 6 (a) Alumina coating, (b) chromia stabilized alumina, and (c) silica coating

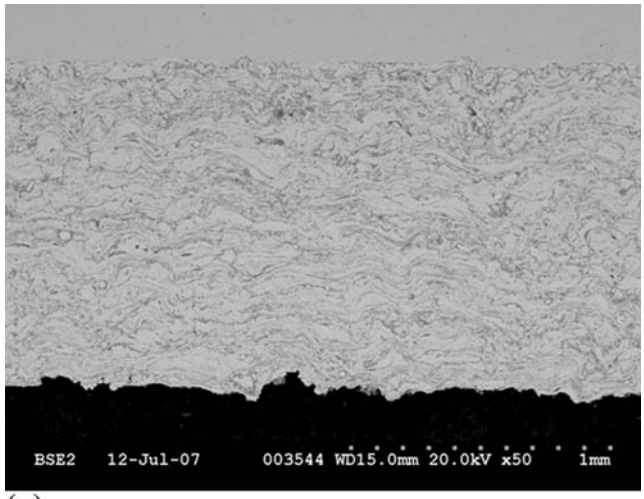

(a)

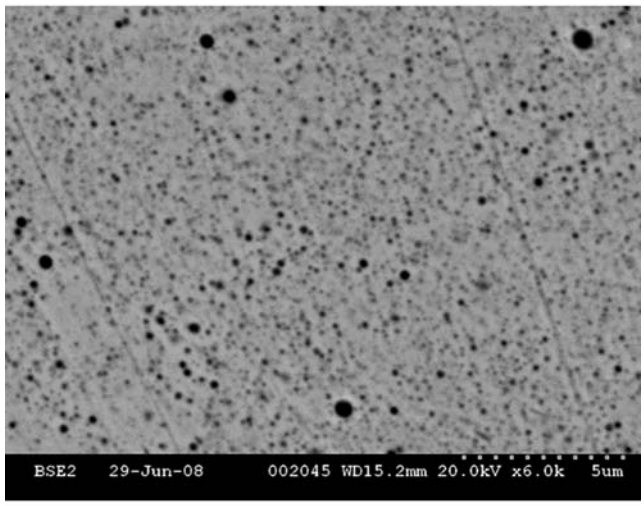

(b)

Fig. 7 (a) SEM picture of NiCr coating with dispersed Al_2O_3 particulates and (b) higher magnification SEM picture of NiCr coating with dispersed Al_2O_3 particulates

Figure 7(a) presents the general cross-sectional microstructure of a NiCr coating with embedded alumina particles produced by the hybrid spray process. The coating is very dense and exhibits the characteristics of an HVOF coating rather than of an arc sprayed coating. The hybrid spray process is unique in the sense that while it yields comparable density to that of the HVOF process, the deposition rate is closer to that of an arc spray process. The observed density is advantageous for high-temperature corrosion and erosion performance of the coatings. Details on the corrosion and erosion performance of the coatings are discussed in the following sections. The dispersion of the alumina particles (dark phase) in the NiCr matrix is shown in Fig. 7(b). As expected, some large particles were present in addition to numerous ultrafine particles. The distribution of the

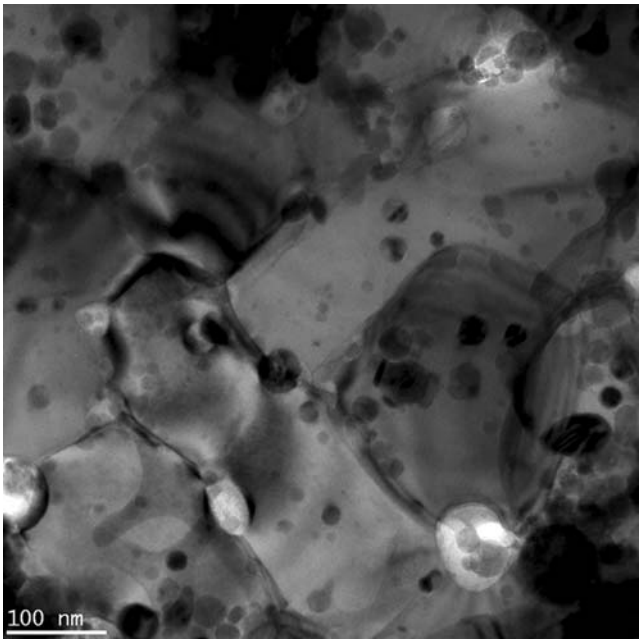

Fig. 8 TEM picture of NiCr coating with dispersed SiO_2 particulates

particles was uniform across the cross section. It is to be noted that composites made from premixed powders commonly exhibit large clusters of nanoparticles. Figure 8 presents the TEM picture of a NiCr coating with embedded silica particles. Many fine particles are observed in the matrix as well as along the grain boundaries. For enhanced creep resistance resulting from grain boundary pinning, the particles must be small and coherent with the matrix. Especially, alloys with very high chrome content can substantially benefit from such ultrafine particle embedment as observed in Fig. 8.

Figure 9 presents the SEM picture for the cross section of a functionally engineered coating with varying particulate embedment following the scheme presented in Fig. 2. The layers closer to the substrate (lower lighter region in the picture) primarily contain silica particles. As the thickness increased, chromia stabilized alumina particles were introduced into the coating in addition to the silica particles. As the particle density increased, the upper part of the picture appeared darker. This composition tailoring during a single deposition step further demonstrates the ability and flexibility of the hybrid concept adopted here. The rational behind this coating design is as follows:

- The silica nanoparticles co-deposited with the NiCr near the substrate interface are expected to provide both creep and spallation resistance (Ref 47).
- The chromia stabilized alumina addition near the working surface of the coating is expected to provide enhanced corrosion, oxidation, and erosion resistance. The silica present in this region can also enhance the oxidation resistance of the alumina and chromia scales.

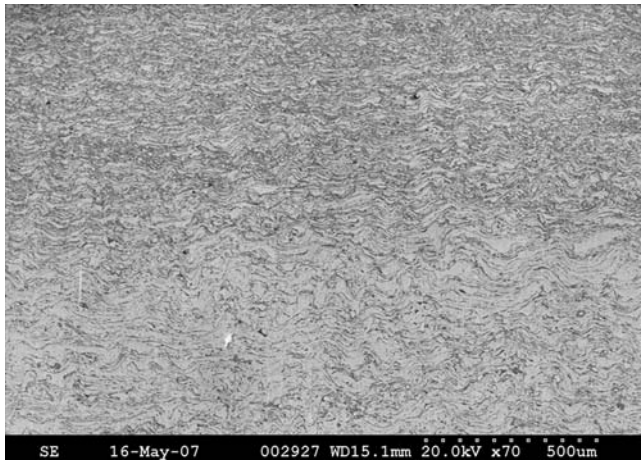

Fig. 9 SEM picture of the FGM coating

The oxidation characteristics of all the coatings (d-h), including the arc sprayed NiCr coating, were investigated by TGA studies in air after removing them from the substrate. The TGA curves shown in Fig. 10 indicate an overall weight gain for all the coatings while heating, although there was an initial weight loss for most samples. The weight gain can be attributed to the oxidation of Cr in the NiCr matrix as well as the changing oxidation state of the existing oxides. The later phenomenon can also lead to a weight loss in the initial stages because of the changing stoichiometry. Literature (Ref 50-55) suggests that the oxidation of chromium during thermal spray processes could lead to nonstoichiometric compounds or metastable oxides (CrO_2, CrO, and Cr_3O_4) which can undergo changes upon reheating. If CrO_2, which has higher oxygen content compared to Cr_2O_3, forms during the spray process, it can undergo stoichiometric changes to a stable oxide (Cr_2O_3) upon reheating and this could lead to an initial weight loss in the coatings. According to Mikkelsen (Ref 56), the specimens may also lose weight due to vaporization of chromium containing species from the chromia scale. Whereas the oxidation of pure Cr to Cr_2O_3 and also the transformation of CrO and Cr_3O_4 to Cr_2O_3 will lead to weight gain because of increasing oxygen content in the coatings. Part of the initial weight loss could also be attributed to the evaporation of moisture absorbed by porosity in the coatings.

The weight gain for arc sprayed NiCr coating was the highest compared to all other coatings and this could be due to the inherent porosity in the arc spray coatings. The pores in the coatings enhance the oxidation rate. The weight gain in the hybrid NiCr coatings (without any particulate) was much lower than the arc sprayed coating because of their dense splat structure. $NiCr + SiO_2$ showed the lowest weight gain. The weight gain by $NiCr + Al_2O_3$ was comparable to that of the plain hybrid NiCr coatings. A large weight gain by the $NiCr + Cr_2O_3$ could be again due to the changes associated in the chromium oxide composition. It is to be noted that there is no need to add Cr_2O_3 particles into NiCr coating using a precursor.

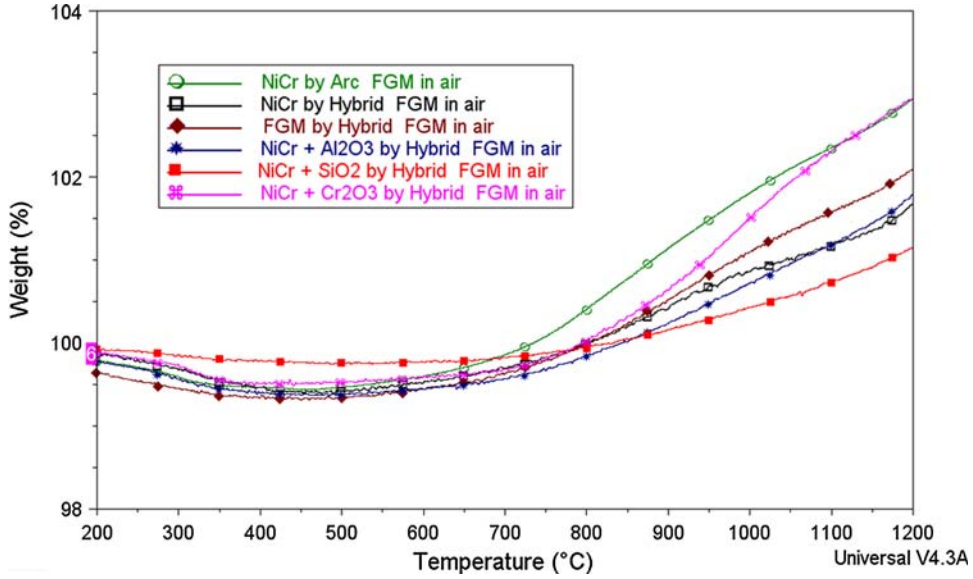

Fig. 10 Weight gain measured using TGA

The role of chromium nitrate precursor here is to stabilize the α-alumina phase. However, excess addition could lead to undesirable consequence as observed in the case of $NiCr + Cr_2O_3$ sample. Determining the appropriate level of the chromium nitrate is beyond the scope of this study. The deleterious effect of excess chromium nitrate is reflected on the weight gain observed in the case of FGM coating which was higher than $NiCr + SiO_2$, $NiCr + Al_2O_3$ and combination. In other words, the beneficial effect of SiO_2 and Al_2O_3 was overshadowed by the complex phases associated with chromia formation form chromium nitrate. From these studies we conclude that addition of SiO_2 has the most remarkable effect on the oxidation behavior of NiCr coatings. It has been demonstrated that the presence of SiO_2 enhances the high-temperature resistance of the chromia scale, which helps to improve the oxidation resistance of the coatings (Ref 44).

3.1 Hot Erosion Test

The setup utilized for evaluating the hot erosion behavior is shown in Fig. 3(a). The weight of cylinders was measured before and after the hot erosion test. Also, the amount of grit used for each test was measured. The measured weight loss of each sample was based on 200 g of grit being used. Samples tested included arc sprayed coatings, plain hybrid coatings, and hybrid coatings with alumina, chromia, and silica, respectively. The results of the tests, shown in Fig. 11, indicate that the hybrid coatings are up to 30% more resistant to erosion than the arc sprayed coatings at 750 °C and this is thought to be due to the higher density of the hybrid coatings. However, the weight loss was slightly higher in the case of oxide particulate embedded coatings. This is contrary to the observation of Xu et al. (Ref 57), who have reported improved erosion resistance with the addition of nanoparticles in Ni-based alloys. Especially, in the case chromia

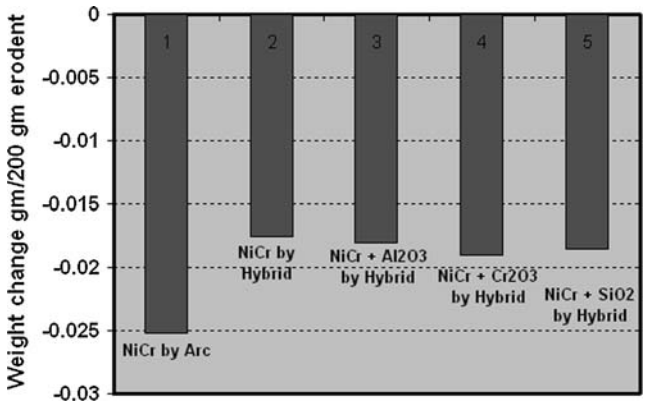

Fig. 11 Weight loss measured hot erosion test

embedment, the difference was noticeable. This may be linked to the large bubble-shaped features with internal voids that were observed in chromia deposit shown in Fig. 6(b).

3.2 Wet Corrosion Test

The corrosion currents measured from the electrochemical tests are shown in Fig. 12. At zero hours, although the hybrid coating showed less current compared to the arc sprayed coating, the difference was not that significant. After 24 h of immersion, the current values significantly differed between the coatings. The arc spray coating measured 2 times greater current, I_0, after 24 h. I_0 is a measure of the corrosion resistance of a material and higher current values indicate lower corrosion resistance. These results confirm that the hybrid coating being denser than the arc spray coating restricts the migration of the corrosive solution/ions to the substrate interface and

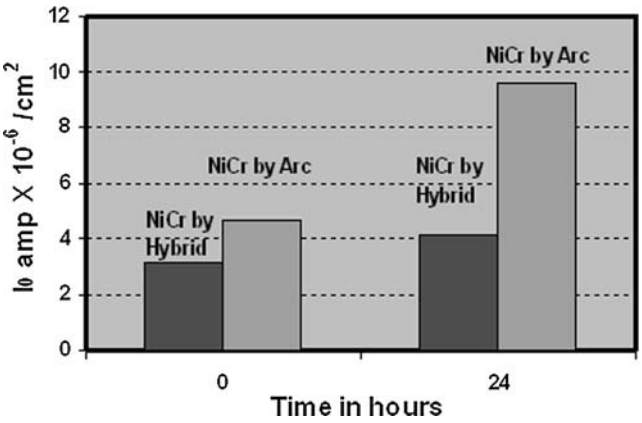

Fig. 12 Wet corrosion of thermally sprayed NiCr coatings in NaCl solution at room temperature

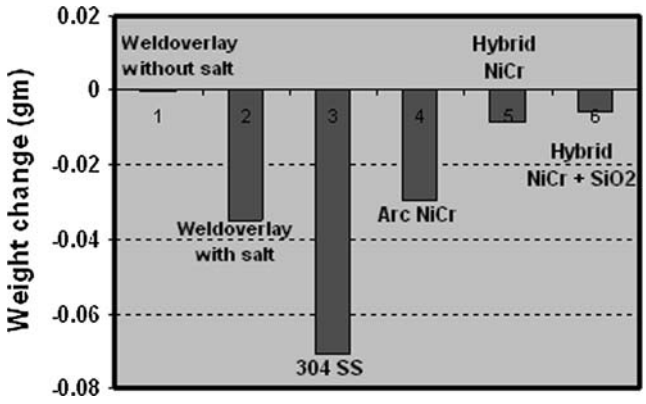

Fig. 13 Weight loss measured hot corrosion test

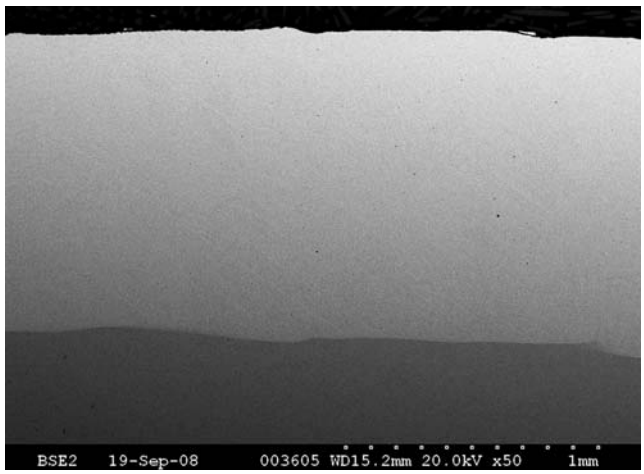

Fig. 14 SEM picture of laser cladded alloy 625 coating

therefore provides more protection to the substrate. Although aqueous corrosion is not an issue for these high-temperature coatings, this test has some significance in terms of molten deposit (sulfates) migration through the coating in coal fired boiler environment.

3.3 Hot Corrosion Test

The hot corrosion test results are shown in Fig. 13. This chart compares the weight loss data obtained on weld overlay coating (with and without salt), 304 stainless steel (304 SS) sample and the coatings—NiCr by arc spray, NiCr and NiCr + SiO_2 by hybrid gun. The chromia stabilized alumina embedded coatings were not included in the test due to their unfavorable oxidation results presented in Fig. 11. NiCr + SiO_2 coatings showed the lowest weight loss compared to all the samples. Plain NiCr coating by hybrid spray also exhibited lesser weight loss compared to the arc spray coating and this could be attributed to the improved density of the hybrid spray coatings. The superior corrosion resistance of the NiCr + SiO_2 coating is possibly due to the enhanced stability of the chromia scale and the improved oxidation resistance caused by SiO_2. Weld overlay coating showed least weight loss in the absence of the salt; however, when salt was present, it showed poor corrosion resistance compared to the hybrid spray coatings.

Although expensive, weld overlay coatings are extensively used in coal fired boiler tubes. Figure 14 shows the superior quality of the laser cladded alloy 625 coating included in this study. The density and homogeneity observed here is not possible in thermal spray coatings. However, the present study demonstrated that even the base NiCr hybrid spray coatings outperformed the alloy 625 coatings in the presence of corrosive salts. The presence of second phase particles, especially SiO_2, showed improved oxidation and corrosion characteristics. Incorporation of ultrafine and nanosized oxide particles is expected to improve the creep properties by pinning the splat boundaries and reducing the oxidation rate. Chromia addition by itself did not help improve the properties significantly; however, it could act as a stabilizer for alumina and limit the phase transformations up to 1200 °C (Ref 46, 58). Combination of SiO_2 and Al_2O_3 can help improve high-temperature creep and corrosion resistance (Ref 44, 59, 60). The creep measurements on hybrid spray coatings are in progress and will be reported elsewhere.

4. Conclusions

Ultrafine oxide particle dispersed NiCr coatings were successfully developed using the ''hybrid spray'' process with simultaneous deposition of NiCr matrix alloy from the wire feed stock and the dispersoids from liquid precursors. The in-flight synthesis of ultrafine particle and simultaneously embedding them into the matrix in a functional manner provides unique capability, reducing the number of steps involved in the synthesis of complex composite coatings which are normally synthesized involving many tedious cost prohibitive steps. Improved density of the hybrid coatings enhanced their high-temperature erosion performance. Thermal analysis of the hybrid coatings

indicated possible formation of non-stoichiometric or metastable oxides. Dispersion of SiO_2 showed marked enhancement in the oxidation and corrosion resistance of the hybrid coatings at high temperatures.

Acknowledgments

This work was supported by NSF STTR grant # 0637748. The authors thank Dr. Terry Ostrom and Elizabeth Shnerpunas for assisting in SEM and AFM imaging of the samples.

References

1. M. Yoshiba, Effect of Hot Corrosion on the Mechanical Performances of Superalloys and Coating Systems, *Corros. Sci.*, 1993, **35**(5-8), p 1115-1121
2. M.A. Uusitalo, P.M.J. Vuoristo, and T.A. Mantyla, High-Temperature Corrosion of Coatings and Boiler Steels Below Chlorine-Containing Salt Deposits, *Corros. Sci.*, 2004, **46**(6), p 1311-1331
3. X.Q. Yu, M. Fan, and Y.S. Sun, The Erosion–Corrosion Behavior of Some Fe_3Al-Based Alloys at High Temperatures, *Wear*, 2002, **253**(5-6), p 604-609
4. P.C. Patnaik, Intermetallic Coatings for High Temperature Applications—A Review, *Mater. Manuf. Processes*, 1989, **4**(4), p 133-152
5. S. Bose, *High Temperature Coatings*, 1st ed., Butterworth-Heinemann Publishers, Boston, 2007
6. D.B. Meadowcroft, High Temperature Corrosion of Alloys and Coatings in Oil- and Coal-Fired Boilers, *Mater. Sci. Eng.*, 1987, **88**, p 313-320
7. A. Martinez-Villafañe, M.F. Almeyara, C. Gaona, J.C. Gonzalez, and J. Porcayo, High-Temperature Degradation and Protection of Ferritic and Austenitic Steels in Steam Generators, *J. Mater. Eng. Perform.*, 1998, **7**(1), p 108-113
8. M.M. Stack, J. Chacon-Nava, and F.H. Stott, Relationship Between the Effects of Velocity and Alloy Corrosion Resistance in Erosion-Corrosion Environments at Elevated Temperatures, *Wear*, 1995, **180**(1-2), p 91-99
9. V. Higuera, F.J. Belzunce, and E. Fernández Rico, Erosion Wear and Mechanical Properties of Plasma-Sprayed Nickel- and Iron-Based Coatings Subjected to Service Conditions in Boilers, *Tribol. Int.*, 1997, **30**(9), p 641-649
10. G.W. Goward, Protective Coatings Purpose, Role and Design, *Mater. Sci. Technol.*, 1986, **2**, p 194-200
11. R. Soltani, T.W. Coyle, and J. Mostaghimi, Microstructure and Creep Behavior of Plasma-Sprayed Yttria Stabilized Zirconia Thermal Barrier Coatings, *J. Therm. Spray Technol.*, 2008, **17**(2), p 244-253
12. D. Zhu and R.A. Miller, Determination of Creep Behavior of Thermal Barrier Coatings Under Laser Imposed Temperature and Stress Gradients, NASA Technical Memorandum 113169, Report Number ARL-TR-1565, 1997
13. M. Niino and S. Maeda, Recent Development Status of Functionally Gradient Materials, *ISIJ Int.*, 1990, **30**(9), p 699-703
14. H.A. Bahr, H. Balke, T. Fett, I. Hoffinger, G. Kirchhoff, D. Munz, A. Neubrand, A.S. Semenov, H.J. Weiss, and Y.Y. Yang, Cracks in Functionally Graded Materials, *Mater. Sci. Eng. A*, 2003, **362**(1-2), p 2-16
15. A.H. Clauer and B.A. Wilcox, The Role of Grain Size and Shape in Strengthening of Dispersion Hardened Nickel Alloys, *Acta Metall.*, 1972, **20**(5), p 743-757
16. L. Xie, E.H. Jordan, N.P. Padture, and M. Gell, Phase and Microstructural Stability of Solution Precursor Plasma Sprayed Thermal Barrier Coatings, *Mater. Sci. Eng. A*, 2004, **381**(1-2), p 189-195
17. M. Roy, A. Pauschitz, J. Wernisch, and F. Franek, The Influence of Temperature on the Wear of Cr_3C_2–25(Ni20Cr) Coating—Comparison Between Nanocrystalline Grains and Conventional Grains, *Wear*, 2004, **257**(7-8), p 799-811
18. J. Liang, W. Gao, Z. Li, and Y. He, Hot Corrosion Resistance of Electrospark-Deposited Al and Ni Cr Coatings Containing Dispersed Y_2O_3 Particles, *Mater. Lett.*, 2004, **58**(6), p 3280-3284
19. Y.C. Kang and S.L. Chan, Tensile Properties of Nanometric Al_2O_3 Particulate-Reinforced Aluminum Matrix Composites, *Mater. Chem. Phys.*, 2004, **85**(2-3), p 438-443
20. U.E. Klotz, R.P. Mason, E. Gohring, and E. Arzt, Estimating Densities of Liquid Transition-Metals and Ni-Base Superalloys, *Mater. Sci. Eng. A*, 1997, **231**(1-2), p 198-205
21. C. Cui, Y. Shen, and F. Meng, Review of Fabrication Methods of In Situ Metal Matrix Composites, *J. Mater. Sci. Technol.*, 2000, **16**(6), p 619-642
22. K.K. Chawla, *Composite Materials—Science and Engineering*, Springer-Verlag Inc., New York, 1998
23. P.K. Rohatgi, R. Asthana, and S. Das, Solidification, Structure and Properties of Metal-Ceramic Particle Composites, *Int. Met. Rev.*, 1986, **31**(3), p 115-139
24. D. Clark, D. Wood, and V. Erb, Industrial Applications of Electrodeposited Nanocrystals, *Nanostruct. Mater.*, 1997, **9**(1-8), p 755-758
25. A. Kawasaki and R. Watanabe, Concept and P/M Fabrication of Functionally Graded Materials, *Ceram. Int.*, 1997, **23**(1), p 73-83
26. E.M. Heian, J.C. Gibeling, and Z.A. Munir, Synthesis and Characterization of Nb_5Si_3/Nb Functionally Graded Composites, *Mater. Sci. Eng. A*, 2004, **368**(1-2), p 168-174
27. S. Suresh and A. Mortensen, *Fundamentals of Functionally Gradient Materials*, The Institute of Materials, University Press, Cambridge, 1999
28. Y. Miyamoto, *Functionally Graded Materials: Design, Processing, and Applications*, Kluwer Academic Publishers, Boston, 1999
29. A. Kawasaki and R. Watanabe, Thermal Fracture Behavior of Metal/Ceramic Functionally Graded Materials, *Eng. Fract. Mech.*, 2002, **69**(14-16), p 1713-1728
30. K.A. Khor, Y.W. Gu, and Z.L. Dong, Mechanical Behavior of Plasma Sprayed Functionally Graded YSZ/NiCoCrAlY Composite Coatings, *Surf. Coat. Technol.*, 2001, **139**(2-3), p 200-206
31. A. Polat, O. Sarikaya, and E. Celik, Effects of Porosity on Thermal Loadings of Functionally Graded Y_2O_3 ZrO_2/NiCoCrAlY Coatings, *Mater. Des.*, 2002, **23**(7), p 641-644
32. L. Prchlik, S. Sampath, J. Gutleber, G. Bancke, and A.W. Ruff, Friction and Wear Properties of WC-Co and Mo-Mo_2C Based Functionally Graded Materials, *Wear*, 2001, **249**(12), p 1103-1115
33. H. Hamatani, N. Shimoda, and S. Kitaguchi, Effect of the Composition Profile and Density of LPPS Sprayed Functionally Graded Coating on the Thermal Shock Resistance, *Sci. Technol. Adv. Mater.*, 2003, **4**, p 197-203
34. K.A. Khor, Y.W. Gu, C.H. Quek, and P. Cheang, Tensile Deformation Behavior of Plasma-Sprayed Ni–45Cr Coatings, *Surf. Coat. Technol.*, 2003, **168**, p 195
35. N.P. Rao, H.J. Lee, M. Kelkar, D.J. Hansen, J.V.R. Heberline, P.H. McMurry, and S.L. Girshick, Nanostructured Materials Production by Hypersonic Plasma Particle Deposition, *Nanostruct. Mater.*, 1997, **9**(1-8), p 129-132
36. G. Skandan, R. Yao, B. Kear, Y. Qiao, L. Liu, and T. Fischer, Multimodal Powders: A New Class of Feedstock Material for Thermal Spraying of Hard Coatings, *Scr. Mater.*, 2001, **44**(8-9), p 1699-1702
37. J.M. Hampikian and W.B. Carter, The Fabrication, Properties and Microstructure of Cu–Ag and Cu–Nb Composite Conductors, *Mater. Sci. Eng. A*, 1999, **267**(1), p 7-18
38. M.R. Hendrick, J.M. Hampikian, and W.B. Carter, Combustion CVD-Applied Alumina Coatings and Their Effects on the Oxidation of a Ni-Base Chromia Former, *J. Electrochem. Soc.*, 1998, **145**(11), p 3986-3994
39. T. Laha, A. Agarwal, T. McKechnie, and S. Seal, Synthesis and Characterization of Plasma Spray Formed Carbon Nanotube Reinforced Aluminum Composite, *Mater. Sci. Eng. A*, 2004, **381**(1-2), p 249-258

40. T. Laha, S. Kuchibhatla, S. Seal, W. Li, and A. Agarwal, Interfacial Phenomena in Thermally Sprayed Multiwalled Carbon Nanotube Reinforced Aluminum Nanocomposite, *Acta Mater.*, 2007, **55**(3), p 1059-1066
41. S.R. Bakshi, V. Singh, K. Balani, D. Graham McCartney, S. Seal, and A. Agarwal, Carbon Nanotube Reinforced Aluminum Composite Coating via Cold Spraying, *Surf. Coat. Technol.*, 2008, **202**(21), p 5162-5169
42. D. Kosikowski, T. Ostrom, and P. Mohanty, Design and Characterization of Simulated Environment Erosion Test Bed, *Proceedings of the International Thermal Spray Conference ITSC06*, 2006, p 1-6 (CD)
43. D. Kosikowski, M. Batalov, and P.S. Mohanty, Functionally Graded Coatings by HVOF-Arc Hybrid Spray Gun, *Proceedings of the International Thermal Spray Conference*, May 2-4, 2005 (Basel, Switzerland), ASM, p 444-449
44. W.B. Carter, J.M. Hampikian, S.H. Godfrey, and T.A. Polley, Thermal Aging of Combustion Chemical Vapor Deposited Oxide Coatings, *Mater. Manuf. Processes*, 1995, **10**(5), p 1007-1020
45. Y. Liu, S. Zha, and M. Liu, Novel Nanostructured Electrodes for Solid Oxide Fuel Cells Fabricated by Combustion Chemical Vapor Deposition (CVD), *Adv. Mater.*, 2004, **16**(3), p 256-260
46. B.R. Marple, J. Voyer, and P. Becharde, Sol Infiltration and Heat Treatment of Alumina–Chromia Plasma-Sprayed Coatings, *J. Eur. Ceram. Soc.*, 2001, **21**, p 861-868
47. P.A. Lessing, R.S. Gordon, and K.S. Mazdiyasni, Creep of Polycrystalline Mullite, *J. Am. Ceram. Soc.*, 1975, **58**(3-4), p 149-150
48. P.C. Dokko, J.A. Pask, and K.S. Mazdiyasni, High-Temperature Mechanical Properties of Mullite Under Compression, *J. Am. Ceram. Soc.*, 1977, **60**(3-4), p 150-155
49. P. Chraska, J. Dubsky, K. Neufuss, and J Pisacka, Alumina Based Plasma Sprayed Materials, Part I: Phase Stability of Alumina and Alumina-Chromia, *J. Therm. Spray Technol.*, 1997, **6**(3), p 320-326
50. M. Vippola, J. Vuorinen, P. Vuoristo, T. Lepisto, and T. Mantyla, Thermal Analysis of Aluminum Phosphate Sealed Plasma Sprayed Oxide Coatings, *J. Eur. Ceram. Soc.*, 2002, **22**(12), p 1937-1946
51. H. Schutz, T. Gossmann, D. Stover, H. Buchkremer, and D. Jager, Manufacture and Properties of Plasma Sprayed Cr_2O_3, *Mater. Manuf. Processes*, 1991, **6**(4), p 649-669
52. L. Hermansson, L. Eklund, L. Askengren, and R. Carlsson, On the Microstructure of Plasma Sprayed Chromium Oxide, *J. Phys.*, 1986, **47**, p C1-C165
53. C. Richard, J. Lu, G. Béranger, and F. Decomps, Study of Cr_2O_3 Coatings Part I: Microstructures and Modulus, *J. Therm. Spray Technol.*, 1995, **4**(4), p 342-346
54. H. Eschnauer, Hard Material Powders and Hard Alloy Powders for Plasma Surface Coating, *Thin Solid Films*, 1980, **73**(1), p 1-17
55. P. Boch, P. Fauchais, and A. Borie, Plasma Spraying with Chromium Oxide, *Proceedings of the 3rd Cimtec International Meeting on Modern Ceramics Technologies*, Rimini, 1997, p 208-211
56. L. Mikkelsen, ''High Temperature Oxidation of Iron-Chromium Alloys,'' Ph.D. Thesis, Risø National Laboratory Roskilde, Denmark, 2003
57. J. Xu, J. Tao, S. Jiang, and Z. Xu, Investigation on Corrosion and Wear Behaviors of Nanoparticles Reinforced Ni-Based Composite Alloying Layer, *Appl. Surf. Sci.*, 2008, **254**(13), p 4036-4043
58. P. Chraska, J. Dubsky, K. Neufuss, and J. Pisacka, Alumina-Base Plasma-Sprayed Materials Part I: Phase Stability of Alumina and Alumina-Chromia, *J. Therm. Spray Technol.*, 1997, **6**(3), p 320-326
59. Y. Liu, C. Compson, and M. Liu, Nanostructured and Functionally Graded Cathodes for Intermediate Temperature Solid Oxide Fuel Cells, *J. Power Sources*, 2004, **138**(1-2), p 194-198
60. D.W. Stollberg, J.M. Hampikian, L. Riester, and W.B. Carter, Nanoindentation Measurements of Combustion CVD Al_2O_3 and YSZ Films, *Mater. Sci. Eng. A*, 2003, **359**(1-2), p 112-118